Ebola virus-induced eye sequelae: a murine model for evaluating glycoprotein-targeting therapeutics

Ha-Na Lee,[a] Biying Xu,[b] Aaron P. Lewkowicz,[a] Kaliroi Engel,[a] Logan Kelley-Baker,[a] Ian L. McWilliams,[a] Derek D. C. Ireland,[a] Jennifer L. Kielczewski,[c] Jinbo Li,[c] Robert N. Fariss,[c] Mercedes M. Campos,[c] Alina Baum,[d] Christos Kyratsous,[d] Kristen Pascal,[d] Chi-Chao Chan,[b] Rachel R. Caspi,[b] Mohanraj Manangeeswaran,[a] and Daniela Verthelyi[a,*]

[a]Division of Biotechnology Review and Research-III, Office of Biotechnology Products, Center for Drug Evaluation and Research, Food and Drug Administration, Silver Spring, MD, 20993, USA
[b]Laboratory of Immunology, National Eye Institute, NIH, Bethesda, MD, 20892, USA
[c]Biological Imaging Core, National Eye Institute, NIH, Bethesda, MD, 20892, USA
[d]Regeneron Pharmaceuticals, Inc., Tarrytown, NY, 10591, USA

eBioMedicine
2024;104: 105170
Published Online xxx
https://doi.org/10.1016/j.ebiom.2024.105170

Summary

Background Ebola virus disease (EVD) survivors experience ocular sequelae including retinal lesions, cataracts, and vision loss. While monoclonal antibodies targeting the Ebola virus glycoprotein (EBOV-GP) have shown promise in improving prognosis, their effectiveness in mitigating ocular sequelae remains uncertain.

Methods We developed and characterized a BSL-2-compatible immunocompetent mouse model to evaluate therapeutics targeting EBOV-GP by inoculating neonatal mice with vesicular stomatitis virus expressing EBOV-GP (VSV-EBOV). To examine the impact of anti-EBOV-GP antibody treatment on acute retinitis and ocular sequelae, VSV-EBOV-infected mice were treated with polyclonal antibodies or monoclonal antibody preparations with antibody-dependent cellular cytotoxicity (ADCC-mAb) or neutralizing activity (NEUT-mAb).

Findings Treatment with all anti-EBOV-GP antibodies tested dramatically reduced viremia and improved survival. Further, all treatments reduced the incidence of cataracts. However, NEUT-mAb alone or in combination with ADCC-mAb reduced viral load in the eyes, downregulated the ocular immune and inflammatory responses, and minimized retinal damage more effectively.

Interpretation Anti-EBOV-GP antibodies can improve survival among EVD patients, but improved therapeutics are needed to reduce life altering sequelae. This animal model offers a new platform to examine the acute and long-term effect of the virus in the eye and the relative impact of therapeutic candidates targeting EBOV-GP. Results indicate that even antibodies that improve systemic viral clearance and survival can differ in their capacity to reduce acute ocular inflammation, and long-term retinal pathology and corneal degeneration.

Funding This study was partly supported by Postgraduate Research Fellowship Awards from ORISE through an interagency agreement between the US DOE and the US FDA.

Keywords: Ebola virus (EBOV); EBOV glycoprotein (EBOV-GP); EBOV-GP pseudotyped vesicular stomatitis virus (VSV-EBOV); BSL-2 model; Anti-EBOV-GP antibodies; Retinitis; Ocular sequelae

Introduction

Ebola virus (EBOV) is a highly virulent single-stranded negative-sense RNA virus belonging to the *Filoviridae* family, notorious for its ability to induce Ebola virus disease (EVD) with a mortality rate of up to 90%.[1,2] Since its initial identification in 1976 near the Ebola River in the Democratic Republic of Congo, numerous outbreaks and epidemics of EBOV have occurred, resulting in tens of thousands of EVD cases and deaths.[3,4] EVD manifests with a range of symptoms and clinical manifestations, including fever, diarrhea, dehydration, malaise, neurological symptoms, systemic hemorrhage, multi-organ failure, shock, and death.[5] Importantly, EVD survivors often have long-term sequelae including arthralgia, cognitive impairment, headaches, hearing loss, myalgia, and ocular complications.[3,6] Ocular

*Corresponding author.
E-mail address: daniela.verthelyi@fda.hhs.gov (D. Verthelyi).

Research in context

Evidence before this study

We searched PubMed with key works "Ebola" and "Eye" for articles published and assessed relevant cited articles. Since Ebola virus disease (EVD) first was identified in 1976, there have been 36 recorded outbreaks, with staggering mortality rates ranging from 35 to 90%. The development of therapeutic monoclonal antibodies targeting EBOV glycoprotein (EBOV-GP), Inmazeb and Ebanga, have reduced mortality, but multiple studies show that EVD survivors can experience life-altering sequelae, including vision loss. Additionally, there is an evidence of long-term EBOV persistence in immune-privileged sites such as the eyes.

Added value of this study

We developed an immune competent BSL-2 compatible model where neonatal C57Bl/6 mice are infected with a replication competent VSV-EBOV that results in high viral titers in the eyes associated with acute retinitis and long-term cataracts. Of interest, as described in patients, surviving mice have detectable viral RNA in the eyes that suggest a low level of persistent viral replication months after the virus is cleared from periphery and become apparently asymptomatic. While this model does not recapitulate every aspect of EVD uveitis and its complications, it provides a platform to assess the performance of therapeutics that target EBOV-GP. Using this model, we examined the impact of anti-EBOV-GP antibody treatment on acute retinitis and long-term ocular sequelae induced by EBOV infection. Our results indicate that although all antibody preparations improved survival, only a combination of anti-EBOV-GP antibodies, which possess neutralizing and ADCC activity, significantly reduces viral load, minimizes retinal damage, and downregulates the immune and inflammatory responses in the eye during acute infection. Further, the long-term ocular sequelae are significantly reduced in mice treated with these anti-EBOV-GP antibodies.

Implications of all the available evidence

Our findings suggest that this immune competent animal model can be used to improve our understanding of EBOV-GP-mediated ocular disease and screen candidate therapeutics targeting EBOV-GP under BSL-2 conditions.

complications leading to vision loss include uveitis, cataract, retinal degeneration, optic neuropathy, hypotony and phthisis bulb.[7,8] Studies conducted on a cohort of EVD survivors in West Africa found that uveitis occurred in 13–34% of cases.[7,8] In addition, EVD survivors exhibited elevated rates of altered intraocular pressure, impairment of color vision, and decreased accommodative tone.[9] One cohort study reported high incidence of ophthalmic complications in the pediatric EVD survivors as compared to the close contact population.[10] In addition, there is mounting evidence of long-term EBOV persistence in immune-privileged sites including the eyes, CNS, and male reproductive tract among EVD survivors, which complicates treatment.[11] This includes a patient who recovered from acute EVD and yet had replicating virus in the aqueous humor 14 weeks after the onset of the disease and 9 weeks after the clearance of viremia, leading to severe unilateral uveitis during convalescence.[12] Additionally, persistent intraocular EBOV RNA was described in an antibody-treated rhesus macaque after clinical resolution, which correlated with severe uveitis.[13] Given the potential public health concerns arising from the long-term ocular complications experienced by EVD survivors and the persistence of the virus in the eyes, there is an urgent need for a research model to assess the effectiveness of anti-EBOV therapeutics in clearing infections and reducing disease severity.

In 2020, FDA approved two antibody-based therapeutics targeting EBOV-GP to treat EVD caused by Zaire ebolavirus in adult and pediatric patients; one is Inmazeb, a combination of three monoclonal antibodies with either neutralizing or ADCC activity targeting different and non-overlapping epitopes on EBOV-GP as well as soluble GP, and the other is Ebanga, a monoclonal antibody against EBOV-GP.[14–16] Both therapeutics reduced disease severity and improved survival among EVD patients when administered early in the disease,[17,18] however, recent studies in non-human primates indicate persistent EBOV infection in the ventricular system of the brain in 7 of 36 rhesus macaques that survived EBOV infection after receiving monoclonal antibody-based treatment.[19] Importantly, their potential in reducing acute ocular infection and long-term ocular complications has not been established.

EBOV is a negative-sense single stranded RNA virus encoding seven genes: nucleoprotein, viral protein 35 (VP35), VP40, VP30, VP24, RNA polymerase and glycoprotein.[20] The EBOV glycoprotein (EBOV-GP) is the sole viral envelop protein and is responsible for cellular attachment, endosomal entry, and membrane fusion to initiate infection, therefore it is a key therapeutic and vaccine target.[21,22] Since EBOV is classified as a biosafety level 4 (BSL-4) virus, research has been hampered by the dearth of facilities, risk, and cost associated with working with animals in high BSL containments, particularly for long-term studies.[23] To overcome the need for BSL-4 facilities, we developed a mouse model of EBOV infection compatible with BSL-2 containment where neonatal mice are subcutaneously inoculated with replicating pseudotyped vesicular stomatitis virus expressing the Zaire EBOV glycoprotein (EBOV-GP) (VSV-EBOV) at postnatal day 3 (P3).[24] These mice develop transient viremia, but the virus localizes

predominantly to the brain and eyes where it infects neurons.[24] Infected animals succumb to the disease 7–12 days post infection (dpi). In the eyes, VSV-EBOV infects neuronal cells in the retina and optic nerve head, resulting in progressive cellular infiltration of the retina and severe disruption of the retinal architecture by 9 dpi together with retinitis, vitritis and choroiditis.[24] Of note, P3 neonatal mice inoculated with VSV pseudovirus expressing Reston EBOV-GP instead of Zaire EBOV-GP did not show signs of disease and survived the challenge, indicating that EBOV disease is dependent on GP.[24]

In a recent study, we used this neonatal mouse model to test the therapeutic effects of SAB-139, a polyclonal anti-EBOV-GP IgG (PolyAb) generated from transchromosomic humanized cows, on EBOV infection in the CNS, and demonstrated that SAB-139 treatment reduces the severity of symptoms, viral load, and inflammatory responses in the CNS and improves the survival.[22] Here, to examine whether we could use this model to test and compare the relative therapeutic effects of different anti-EBOV-GP therapeutics on EBOV-induced acute retinitis and long-term ocular sequelae, we used four antibody preparations: a polyclonal antibody (PolyAb; SAB-139), an antibody-dependent cell cytotoxicity (ADCC)-mediating non-neutralizing monoclonal antibody (ADCC-mAb; REGN3478), a neutralizing monoclonal Ab without ADCC (NEUT-mAb; REGN3481), and a combination of REGN3478 and REGN3481 (ADCC-mAb + NEUT-mAb).

Methods

Ethics

The animal experimental protocol 2016–13 was reviewed and approved by the FDA Animal Care and Use Committee (FDA-ACUC), and all animals used in these studies conform to relevant regulatory standards. All procedures were performed in accordance with the FDA ACUC guidelines.

Mice

C57BL/6J (B6) mice were purchased from Jackson Laboratory. Naïve three-day-old (P3) neonatal mice born from specific pathogen-free parents were randomly split into groups for use in this study and these mice were not separated by sex, as sex assignment is difficult before day 15. Mice were bred and housed in the FDA AAALAC accredited, pathogen-free animal facility. Mice were housed in standard cages with 1 breeding pair or up to 5 single sex mice per cage and a 12/12 light/dark schedule and fed on commercial 5P76 Prolab Isopro RMH 3000 diet. Animal studies were reported according to ARRIVE guidelines, and no animals were excluded from the study.

Pseudotyped viruses

As described in McWilliams IL et al.,[24] we obtained the VSV-G-deleted Vesicular Stomatitis Virus containing the Zaire (Mayinga) Ebolavirus glycoprotein (VSV-EBOV) from BEI Resources (established by NIAID and maintained by ATCC). Viral stocks were passaged in Vero E6 cells to produce a master stock and stored at –80 °C. Viral quantification of stocks was performed by $TCID_{50}$.

Cell lines

VERO E6 kidney epithelial cell-line was purchased from ATCC (Cat. CRL-1586; RRID:CVCL_0574) and cultured in MEM media containing 10% fetal bovine serum (FBS), 1% Pen-Strep, and 1% L-Glutamine in a 37 °C, 5% CO_2 incubator for the duration of culture. Prior to each cell-based experiment, cell morphology and viability were assessed for cell validation.

Neutralization assay

VERO E6 cells were seeded at 3×10^4 cells/well in 96 well plates to a target confluency of 70–90% at 24 h after plating. VSV-EBOV (MOI 0.1) was incubated with serial antibody dilutions for 1 h at 37 °C. Antibody-virus complexes were added to VERO E6 cell monolayers in 96-well plates and incubated at 37 °C for 1 h. Subsequently, the cells were washed, and incubated for 5 days in fresh media. Neutralizing ability of antibodies was assessed by monitoring levels of cytopathic effect and compared to untreated control wells using an Olympus IX-81 microscope.

Mouse infections and treatments

Viral stocks were diluted to working concentration to administer 1000 $TCID_{50}$ of virus in 50 µl sterile phosphate buffer solution subcutaneously (s.c) in the scruff of the neck of P3 neonatal mice using a 31-gauge needle. SAb Biotherapeutics (Sioux Falls, SD) and Regeneron Pharmaceuticals (Tarrytown, NY) kindly provided us SAB-139, REGN3478 and REGN3481, respectively. Stocks were diluted to 10 mg/ml in saline and administered intraperitoneally (i.p.) at 100 mg/kg (for combination regimen, 50 mg/kg of each antibody) in mice at 3 dpi. Mice that were determined to be moribund per criteria pre-established in the protocol by laboratory or animal-care staff were euthanized and counted as dead. Mice that were euthanized to collect eyes were exsanguinated by perfusion with cold PBS. TCID50 assay and histology were conducted using the left eye from each mouse, while immunohistochemistry and RNA isolation were performed on the right eye. For flow cytometry analysis, cells from both eyes were pooled.

Complete blood count

Blood samples were collected from mice at 9 dpi by drawing 100 µl into EDTA-containing tubes. The CBC analysis was performed within 30 min of blood collection by using the Element HT5 veterinary hematology analyzer (Heska, Loveland, CO). The reference range for lymphocytes in mice is typically between 600 and

8900 cells per microliter, with lymphopenia defined as lymphocyte counts below 600 cells per microliter.

$TCID_{50}$ viral quantification

VERO E6 cells were plated in 100 µl of complete MEM media in a 96 well plate to a target confluency of 70–90% at 24 h after plating. Eyes were homogenized and cleared of cellular debris by centrifugation. The cleared supernatant was then serially diluted in non-supplemented MEM media and 100 µl/well was plated in the VERO E6 96 well plate. Cytopathic effect was read 4–5 days after inoculation and $TCID_{50}$ was calculated as previously described.[25]

Eye histopathology and imaging

Infected mice were euthanized at 9 dpi or 3 months post infection (mpi) and perfused with sterile PBS. The left eye from each mouse was fixed in formalin at 4 °C until being embedded in methacrylate. The eyes were serially sectioned in 10 µm along the pupillary-optic nerve plane and then stained with hematoxylin and eosin (H&E). The severity of retinal inflammation and damage was scored on a scale of 0–4 by a blinded ophthalmic pathologist as previously described.[26] For immunocytochemistry, the right eye from each mouse was fixed in 4% paraformaldehyde for 2 h at room temperature and washed in PBS. The anterior segment and lens were dissected and the posterior eye cups containing the retina were cryoprotected in increasing concentrations of sucrose (10%–30%) in 1× PBS. Eye cups were embedded in Tissue-Tek O.C.T. (Sakura-Finetek, Torrance, CA) and frozen with Histo-Cyto Freeze (Ted Pella, Redding, CA). The tissue blocks were stored at –80 °C until cryosectioned. A Leica cryostat was used to collect 10 µm frozen sections which were placed on SuperFrost Plus slides (Fisher Scientific, Carlsbad, CA). Frozen retinal sections were dried under vacuum for 30 min. Sections were encircled with a hydrophobic ImmunEdge barrier (Vector Labs), and permeabilized with ICC buffer (1× PBS + 0.5% BSA + 0.2% Tween-20 + 0.05% sodium azide pH 7.30). Sections were incubated overnight at 4 °C with the following antibodies: anti-Ebola GP antibody conjugated to Alexa Fluor (AF) 568 (1:250) (clone: KZ52; Absolute antibody, Boston, MA, cat. Ab00690-23.0), anti-NF-160 antibody conjugated to AF488 (1:250) (Sigma, St. Louis, MO, cat. N5264-100 µl (Sigma–Aldrich, St. Louis, MO, cat. N5264, RRID:AB_477278), anti-IBA-1 antibody conjugated to AF635 (1:500) (Wako Chemicals, Lexington, MA, cat. 018-28523, RRID:AB_2936184) and, anti-CD45 antibody conjugated to AF488 (1:250) (BioLegend, San Diego, CA, cat. 103122, RRID:AB_493532). Antibodies were validated in the lab by testing different antibody clones and dilutions to optimize signal-to-noise ratio and to ensure accurate identification of cellular markers. DAPI (ThermoFisher Scientific, Carlsbad, CA, cat. P36941) was included at 1:500 dilution in all immunolabeled samples to label nuclei. Sections were washed with ICC buffer 3 × 15 min and 1 × 30 min. FluoroGel (Electron Microscopy Sciences, Hatfield, PA) was applied to sections before coverslipping to retard photobleaching. ApopTag Fluorescein in situ apoptosis detection kit (Millipore, Massachusetts, USA, cat. S7110EA-MIL) was used to detect cells undergoing apoptosis. Sections were imaged on a Nikon A1R resonance scanning confocal microscope (Nikon Instruments, Melville, NY) using a 25 × 1.05NA PlanApo Silicone oil objective. Image files were coded, and then examined blindly by an ocular pathologist. The number of $TUNEL^+$ cells were counted using Image-J software (http://imagej.nih.gov/ij) and expressed per field of view. Three different fields per section was used to count the number of $TUNEL^+$ cells.

Flow cytometry

Eyes were enucleated and the tissue around the eye except the optic nerve and lenses were removed. The remaining tissue was minced in RPMI1640 (Gibco, Billings, MT) and incubated with 1 mg/ml collagenase D (Roche, Indianapolis, IN, cat. 11088858001) for 45 min at 37 °C. Cells were then dispersed by trituration using a pipette, washed, filtered through 40 µm cell strainer, and resuspended in RPMI supplemented with 10% FBS. Isolated cells were stained with a cocktail of antibodies against various lineage markers, including CD45 (BioLegend, cat. 103149, RRID:AB_2564590), F4/80 (BioLegend, cat. 123120, RRID:AB_893491), CD11b (BioLegend, cat. 101257, RRID:AB_2565431), CD11c (BioLegend, cat. 117318, RRID:AB_493569), Ly6G (BioLegend, cat. 127633, RRID:AB_2562937), NK1.1 (BD Bioscience, cat. 557391, RRID:AB_396674), CD3 (BioLegend, cat. 100351, RRID:AB_2565842), CD4 (BD Bioscience, cat. 553052, RRID:AB_394587) and CD8 (BioLegend, cat. 100729, RRID:AB_493702). Antibodies were validated by testing different antibody clones to optimize signal-to-noise ratio and to ensure accurate identification of cellular markers. Flow cytometry data were collected with the BD LSRFortessa X-20 flow cytometry (BD Biosciences, San Jose, CA), and the results were analyzed using FlowJo software (version 10.8.1).

RNA extraction

After perfusion, the eyes were collected into Trizol (ThermoFisher Scientific, cat. 15596026) from infected animals at 9 dpi and stored at –80 °C until RNA was isolated (per Trizol manufacturers' protocol). RNA concentration and purity were determined by spectrophotometry at 260 nm and 280 nm using a NanoDrop 1000 spectrophotometer (ThermoFisher Scientific).

Gene expression analysis

mRNA expression levels of immune-related genes were determined using the Nanostring nCounter gene expression system (NanoString Technologies, Seattle, WA). Isolated RNA (100 ng) was hybridized with probes from nCounter Mouse Inflammation v2 Panel at 65 °C

for 18 h. Hybridized products were prepared for cartridge loading on an nCounter PrepStation. Digital Counting of fluorescent signals was conducted using the nCounter Digital Analyzer. Data analysis including statistics was carried out with the nSolver 4.0 software.

Virus quantification by real-time qPCR

One microgram (μg) of isolated total RNA was analyzed to establish VSV nucleocapsid (VSV-N) RNA levels, which are expressed as VSV-N copies/μg. Absolute quantification was determined using genomic viral RNA transcribed from a plasmid using the T7 Megascript transcription kit (ThermoFisher Scientific, cat. AM1333). The number of copies was calculated based on absorbance at 260 nm. One-step reverse transcription (RT)-real time qPCR was performed on a 10-fold serial dilution of this standard RNA in parallel with 1 μg of unknown sample RNA. This assay amplifies VSV genome position 1083–1144 based on wild type VSV (Indiana serotype)[27] in a single tube using 25 μl reaction volume (RNA to cDNA kit, ThermoFisher Scientific). Reaction parameters for the Applied Biosystems Viia7 real time PCR machine: 60 °C for 30 min for reverse transcription, followed by 95 °C for 15 min to inactivate the RT enzyme and activate the DNA polymerase followed by 45 cycles of 95 °C, 15 s and 60 °C for 1 min. Detection of positive-and negative-sense strands of VSV-N was performed in a 2-step real-time PCR reaction. Briefly, reverse transcription of total RNA isolated from eyes was performed using T7-or GVA-tagged VSV-N-specific primers and Oligo d(T)16 primers (ThermoFisher Scientific) for first-strand synthesis (High-Capacity cDNA reverse transcription kit, ThermoFisher Scientific). These reactions synthesized T7-tagged positive-sense and GVA-tagged negative-sense viral cDNA. The resulting cDNA was amplified using qPCR with forward primers binding to the strand-specific Tags (T7 or GVA) and reserve primers were specific to the VSV-N gene sequences. A common Taqman probe specific for the VSV-N amplicon was used to detect amplified cDNA. All custom primer/probes in this assay were produced by Eurofins Genomics, USA (sequences are listed in the Supplementary Table S1). As no standard curve was available for both strands, relative levels normalized to GAPDH are expressed.

Fundus examination

Mice were anesthetized by i.p. injection of ketamine/xylazine and were dosed based on body weight. Mice were kept warm by using heat pads or heat lamps. Immediately after injecting anesthetic, one drop each of phenylephrine hydrochloride ophthalmic solution (2.5%) and Tropicamide ophthalmic solution (0.5%) was added to each eye to dilate the pupil and facilitate imaging of the retina. A digital camera connected to an endoscope (Karl Storz, Germany) for taking pictures of mouse fundus was used. A drop of hypromellose ophthalmic demulcent solution (2.5%) was applied to the cornea before flattening the eye slightly to view the fundus through the fundoscope. After the exam, a drop of polyvinyl alcohol (1.4%) was placed on each eye to keep the eyes moist.

Statistical analysis

Comparisons between groups used the 2-tailed unpaired Student's t test or ANOVA as appropriate; *P*-values were adjusted for multiple comparisons as appropriate. Differences in weight were analyzed by a two-way ANOVA (mixed effects model with the Geisser-Greenhouse correction). Survival curves were tested using the Log-rank (Mantel–Cox) test. Statistical analyses were conducted with GraphPad Software (version 10.0.0). Adjusted $P < 0.05$ was considered statistically significant.

Role of funders

The funding sources did not have any role in study design, data collection, data analysis, interpretation or writing of this manuscript.

Results

Anti-EBOV-GP antibody treatment protects mice from VSV-EBOV-induced death

Our previous study demonstrated that a subcutaneous challenge of 3-day old C57BL/6 mice with VSV-EBOV pseudovirus (1000 $TCID_{50}$; s.c.) results in a lethal meningoencephalitis.[24] To examine if anti-EBOV-GP antibodies would control viral infection in this neonatal mouse model of EBOV infection, we tested four antibody preparations that target EBOV-GP: SAB-139 (PolyAb), a polyclonal antibody manufactured in transchromosomic cows, a mAb with ADCC activity (REGN3478; ADCC-mAb) (Supplementary Figure S1), a mAb with neutralizing activity (REGN3481; NEUT-mAb) and the combination of REGN3478 and REGN3481 (ADCC-mAb + NEUT-mAb). *In vitro*, polyAb and the combination of ADCC-mAb and NEUT-mAb exhibited stronger neutralization compared to NEUT-mAb alone while, as expected, ADCC-mAb did not show neutralization capacity (Fig. 1a). Both polyAb and the combination of ADCC-mAb and NEUT-mAb completely blocked the viral activity at 1 nM (Fig. 1a). To examine whether our neonatal mouse model could be used to test different therapeutics targeting the EBOV-GP, neonatal mice challenged on P3 with VSV-EBOV (1000 TCID50) were treated intraperitoneally (i.p.) at 3 dpi with poly-IgG (100 mg/kg), ADCC-mAb (100 mg/kg), NEUT-mAb (100 mg/kg) or the combination of ADCC-mAb and NEUT-mAb (50 mg/kg, each). Control mice received IgG isotype controls (100 mg/kg) at 3 dpi. Consistent with previous reports,[22,24] mice infected with VSV-EBOV showed reduced weight gain and about 90% of them succumbed to the disease at 7–12 dpi (Fig. 1b and c). Moreover, as observed in EBOV-infected patients,[28] all VSV-EBOV-infected mice

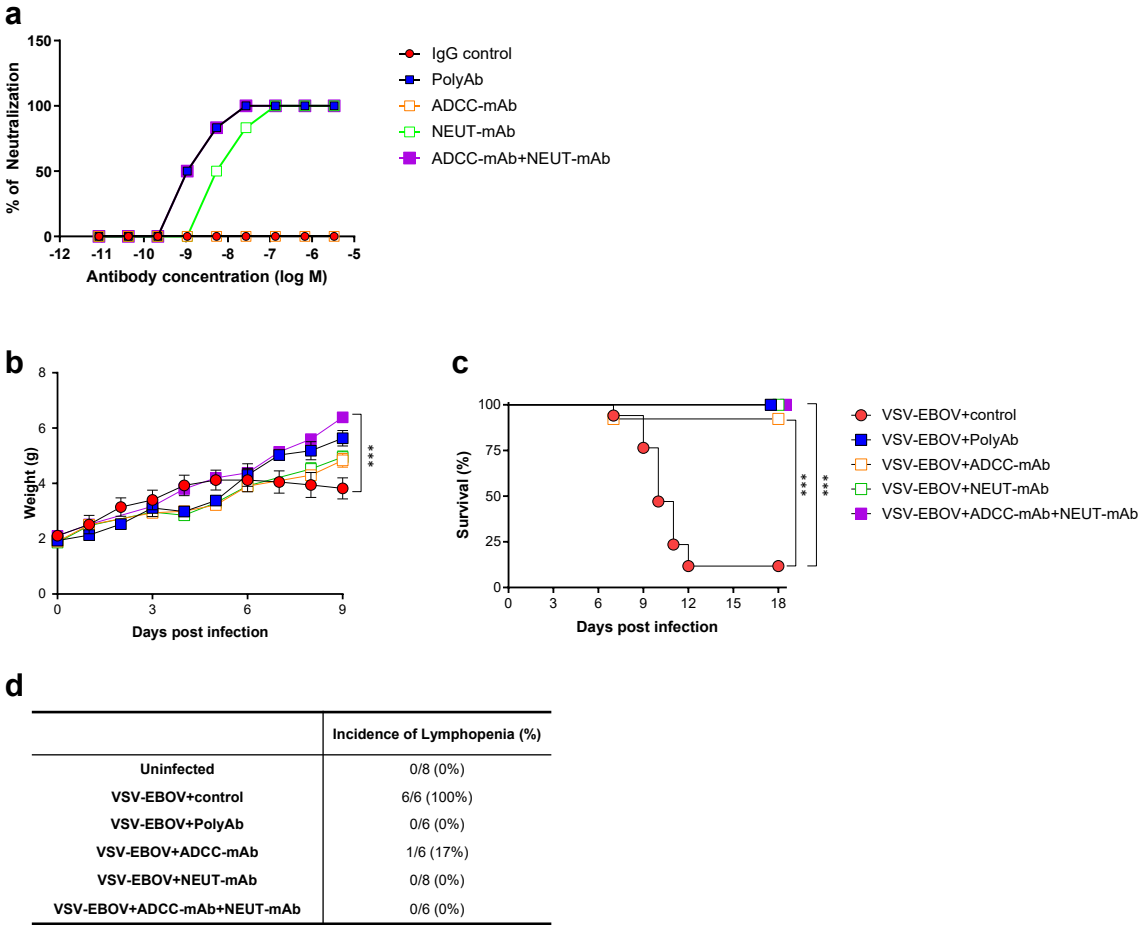

d

	Incidence of Lymphopenia (%)
Uninfected	0/8 (0%)
VSV-EBOV+control	6/6 (100%)
VSV-EBOV+PolyAb	0/6 (0%)
VSV-EBOV+ADCC-mAb	1/6 (17%)
VSV-EBOV+NEUT-mAb	0/8 (0%)
VSV-EBOV+ADCC-mAb+NEUT-mAb	0/6 (0%)

Fig. 1: **Therapeutic effects of anti-EBOV-GP antibodies on weight change, survival and lymphopenia in VSV-EBOV-infected mice. (a)** Virus neutralization by antibodies: SAB-139 (polyAb), REGN3478 (ADCC-mAb), and REGN3481 (NEUT-mAb) or the combination of ADCC-mAb and NEUT-mAb using VERO E6 cells infected with replicating VSV-EBOV (MOI 0.1). Data are representative of three independent experiments. **(b–d)** P3 C57BL/6 mice were subcutaneously (s.c.) infected with 1000 TCID50 of VSV-EBOV and intraperitoneally (i.p.) treated with human IgG isotype controls (IgG control; 100 mg/kg, (b) n = 9, (c) n = 17, or (d) n = 6, respectively), polyAb (100 mg/kg, (b) n = 3, (c) n = 12, or (d) n = 6), ADCC-mAb (100 mg/kg, (b) n = 10, (c) n = 13, or (d) n = 6), NEUT-mAb (100 mg/kg, (b) n = 8, (c) n = 12, or (d) n = 8) or the combination of ADCC-mAb and NEUT-mAb (50 mg/kg, each, (b) n = 11, (c) n = 10, or (d) n = 6) at 3 dpi. Mice were monitored for weight changes **(b)** and survival **(c)**. Data are shown as mean ± standard deviation (SD). Statistical significance was determined using a two-way ANOVA (mixed-effects model with the Geisser-Greenhouse correction) **(b)** and the log-rank test **(c)**, respectively. ***$P < 0.001$ compared to infected mice treated with IgG control. **(d)** Hematological assessment at 9 dpi. Table shows incidence of lymphopenia by 9 dpi.

developed significant lymphopenia by 9 dpi (Fig. 1d). Treatment with anti-EBOV-GP antibodies, including non-neutralizing antibody ADCC-mAb, albeit to a lesser extent, successfully normalized weight gain and lymphocyte counts, and improved survival (Fig. 1b–d). These data suggest that both neutralizing activity and effector function may have mutually exclusive roles in conferring protection as all of these antibodies reduced morbidity and mortality in EBOV infection.

Anti-EBOV-GP antibody treatment reduces virus load in the eyes

VSV-EBOV infects retinal neurons of newborn mice causing a progressive disruption of the retinal architecture.[24] As previously reported, the eyes of VSV-EBOV-infected mice that received IgG control Abs showed progressive increase in viral loads starting at 3 dpi (Fig. 2a), and viral antigens were evident in neuronal cells in the outer nuclear layer (ONL) of the retina, and to a lesser degree in the inner nuclear layer (INL) by 9 dpi (Fig. 2b). Although all the treatments improved survival and reduced viremia (Supplementary Figure S2), the anti-EBOV-GP antibodies differed in their ability to clear the virus from the eye. As shown in Fig. 2a and b, administration of NEUT-mAb appeared to be more effective in reducing the viral load in the eye than polyAb or ADCC-mAb. Of note, while viral clearance was minimal when using non-neutralizing

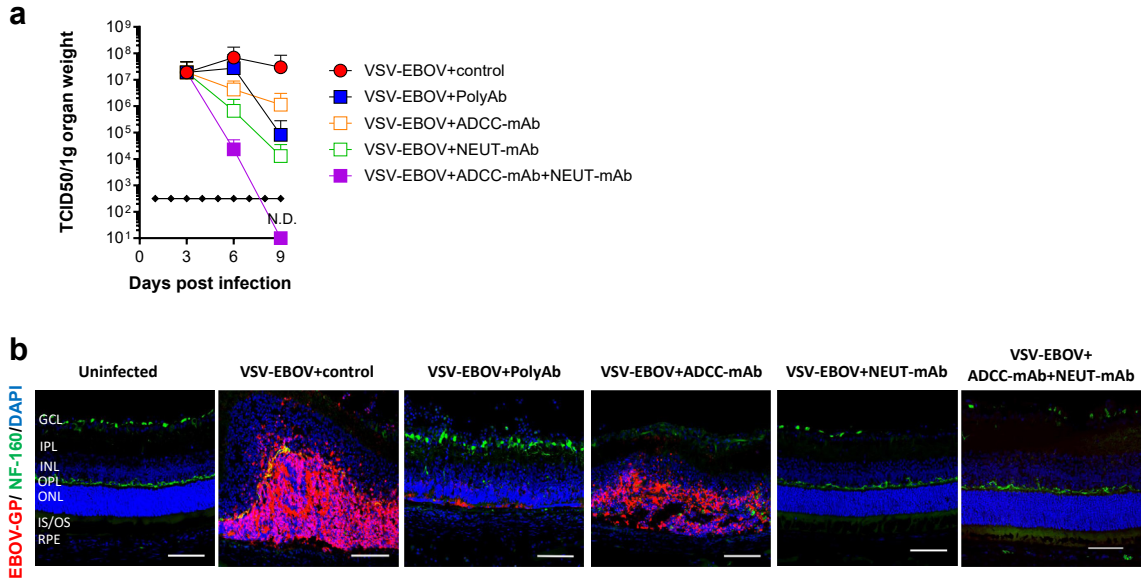

Fig. 2: **Viral burden in the eyes of VSV-EBOV-infected mice treated with anti-EBOV-GP antibodies**. P3 C57BL/6 mice were infected s.c. with 1000 TCID50 of VSV-EBOV and treated IgG control (100 mg/kg, (a) n = 5 or (b) n = 6), polyAb (100 mg/kg, (a) n = 6 or (b) n = 3), ADCC-mAb (100 mg/kg, (a) n = 3 or (b) n = 6), NEUT-mAb (100 mg/kg, (a) n = 3 or (b) n = 4) or the combination of ADCC-mAb and NEUT-mAb (50 mg/kg, each, (a) n = 3 or (b) n = 5) at 3 dpi. **(a)** Viral loads in the eyes of mice were evaluated by TCID50 at 3, 6 and 9 dpi. Data are shown as mean + SD. N.D., not detectable. **(b)** Viral antigen in the eyes of uninfected mice (n = 5) and VSV-EBOV-infected mice treated as above at 3 dpi and sacrificed at 9 dpi. The images show representative immunofluorescence images of eye sections stained for EBOV-GP antigen (red), NF-160 (green) and DAPI (blue). Scale bar: 50 µm. GCL, ganglion cell layer; IPL, inner plexiform layer; INL, inner nuclear layer; OPL, outer plexiform layer; ONL, outer nuclear layer; IS/OS, inner/outer segment junction; RPE, retinal pigment epithelium. Images of the full eye can be found in Supplementary Figure S6.

ADCC-mAb, co-treatment with ADCC-mAb and NEUT-mAb was more effective than any of the individual preparations (Fig. 2a and b).

Anti-EBOV GP antibodies reduce VSV-EBOV-induced ocular pathology to different degrees

Having established that anti-EBOV GP antibodies reduces the viral load in the eyes of VSV-EBOV-infected mice, we next investigated whether this is associated with reduced ocular pathological findings. In agreement with our previous report,[24] VSV-EBOV-infected mice showed progressive retinitis, choroiditis, vitritis, retinal destruction/degeneration, and retinal edema by 9 dpi (Fig. 3a). All the histological features of ocular damage were reduced following treatment with anti-EBOV GP antibodies, albeit to different degrees. Mice treated with NEUT-mAb or ADCC-mAb + NEUT-mAb did not show severe retinal inflammation or architectural disruptions (retinal inflammation score ≤2), while 30 and 50% of infected mice treated with polyAb or ADCC-mAb showed severe retinal inflammation, respectively (Fig. 3a). Indeed, along with insufficient viral clearance, treatment with ADCC-mAb alone failed to mitigate retinitis, retinal vasculitis, choroiditis, vitritis, and retinal disorganization, and consequently, the retinal inflammation scores remained high and comparable to those of infected mice treated with IgG controls (Fig. 3a). Immunohistochemistry analysis confirmed that treatment with NEUT-mAb or ADCC-mAb + NEUT-mAb lessened retinal inflammation and destruction as evident by reduced $CD45^+$ infiltrating cells and $TUNEL^+$ apoptotic cells compared to IgG controls (Fig. 3b and c). In addition, polyAb treatment did not reduce cellular apoptosis or immune cell infiltration in the retina (Fig. 3b and c). Similarly, mice treated with ADCC-mAb showed no significant reduction in the level of apoptotic cells, and only 3 out of 6 mice showed reduction in $CD45^+$ infiltrating cells (Fig. 3b and c). Failure to reduce immune cell infiltration by polyAb treatment was confirmed by flow cytometry analysis (Fig. 3d and Supplementary Figure S3). T cells were found to be the predominant infiltrating cells in the eyes 9 days after a VSV-EBOV challenge and remained the main type of infiltrating cell regardless of anti-EBOV-GP treatment at 9 dpi (Fig. 3d and Supplementary Figure S3). Treatment with ADCC-mAb, NEUT-mAb or their combination significantly reduced cellular infiltration into the eyes, however, polyAb-treated mice exhibited high proportion of $CD45^+$ and T cells in the eyes, comparable to IgG control-treated animals (Fig. 3d and Supplementary Figure S3). Our previous study demonstrated that although polyAb treatment reduces viral load and inflammation in the brain of VSV-EBOV-infected mice,

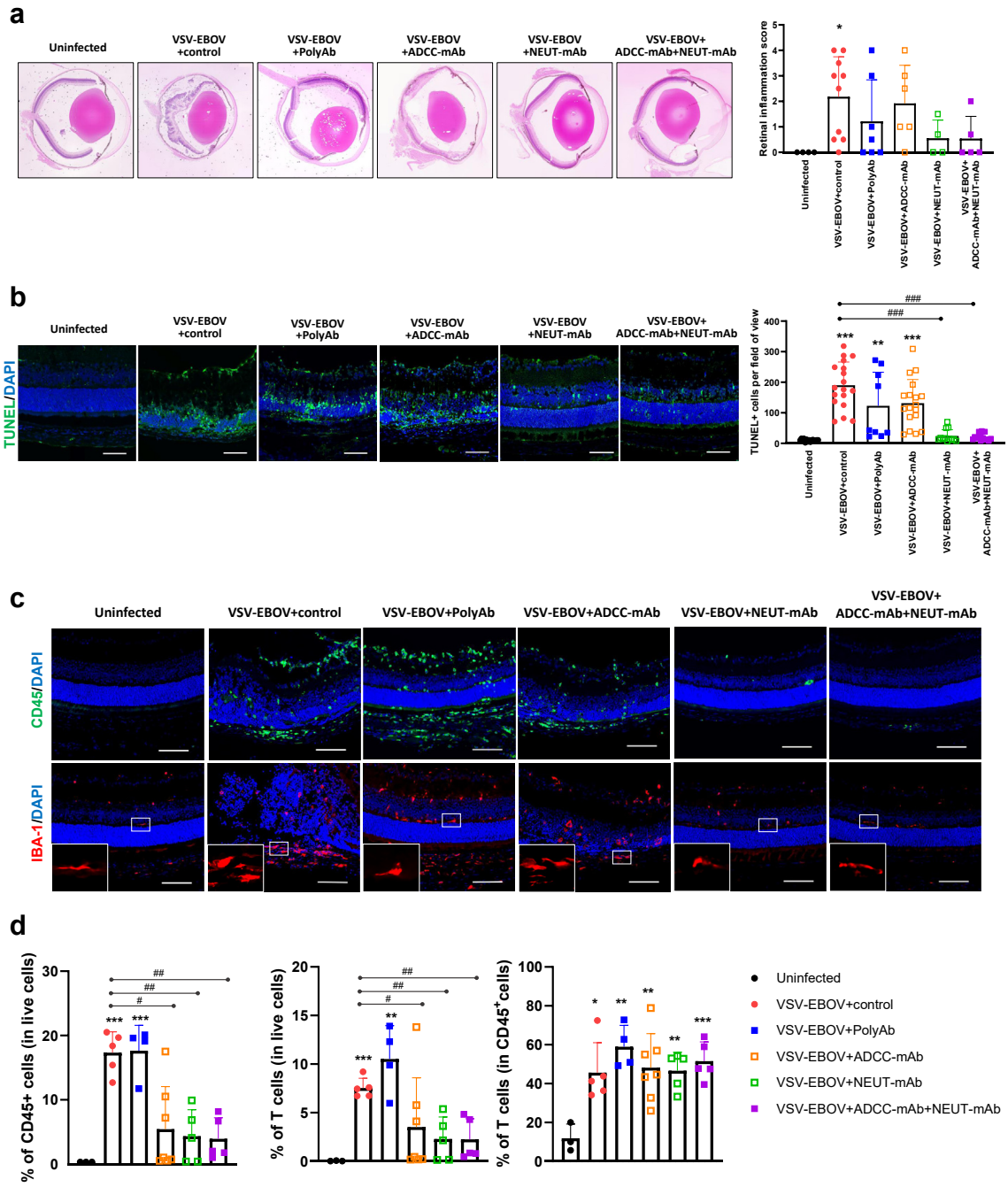

***Fig. 3*: Therapeutic effects of anti-EBOV-GP antibodies on acute retinal inflammation in VSV-EBOV-infected mice**. P3 C57BL/6 mice were infected, treated as above at 3 dpi, and sacrificed at 9 dpi. **(a)** Histopathology of the eyes of uninfected mice (n = 4) and VSV-EBOV-infected treated with IgG control (n = 10), polyAb (n = 7), ADCC-mAb (n = 6), NEUT-mAb (n = 4) or the combination of ADCC-mAb and NEUT-mAb (n = 5). Left images show representative H&E staining of eyes. Right graph shows the retinal inflammation score. Data are shown as mean + SD. **(b)** Left images show representative immunofluorescence staining for TUNEL (green) and DAPI (blue) in eye sections from uninfected mice (n = 5) and VSV-EBOV-infected mice treated with IgG control (n = 6), polyAb (n = 3), ADCC-mAb (n = 6), NEUT-mAb (n = 4) or the combination of ADCC-mAb and NEUT-mAb (n = 5). Scale bar: 50 µm. Images of the full eye can be found in Supplementary Figure 6. Right graph shows the quantification of TUNEL + cells per field of view (3 fields per eye section). Data are shown as mean + S.D. (n = 9–18 fields for each group). **(c)** The images show representative immunofluorescence staining for CD45 (green), IBA (red) and DAPI (blue) in eye sections from uninfected mice (n = 5) and VSV-EBOV-infected mice treated with IgG control (n = 6), polyAb (n = 3), ADCC-mAb (n = 6), NEUT-mAb (n = 4) or the combination of ADCC-mAb and NEUT-mAb (n = 5). The bottom close-up images show representative microglia morphology observed in

it fails to prevent microglial activation when administered after the virus is established in the brain.[22] Here, we also observed the increased number of IBA$^+$ cells with amoeboid morphology, indicative of activated microglia in the retina of VSV-EBOV-infected mice (Fig. 3c). Interestingly, polyAb and ADCC-mAb treatment at 3 dpi failed to attenuate microglial activation in the eyes as evident by increased IBA expression and morphological changes (Fig. 3c). However, microglia in the eyes of infected mice treated with NEUT-mAb or ADCC-mAb + NEUT-mAb appear comparable to ones observed in uninfected mice (Fig. 3c).

Anti-EBOV GP antibody treatment reduces overall inflammatory profile in the eyes following VSV-EBOV challenge

Uncontrolled inflammation is regarded as a hallmark of EVD. Studies conducted on rhesus monkeys infected with EBOV show elevated levels of pro-inflammatory cytokines in the vitreous fluid.[13] In this study, assessment of mRNA expression in the eyes of the infected mice showed increased expression of genes associated with recruitment and activation of T and NK cells (e.g. *Gzm, Cd3, Klrc1, Klrd1, Klrk1, Il2r, Cxcl10* and *Ccl5*), activation of antigen presenting cells (e.g. *Mhc, Ciita, Clec4e, Ccl2, Cd74, Ccl5* and *Cxcr6*), and interferon responses (e.g. *Ifna1, Ifnb1, Ifng, Ifi204, Irgm1, Irf7 and Slamf7*) (Fig. 4). Consistent with the reduced viral load and cellular infiltration, mice treated with the combination of ADCC and NEUT-mAbs and to a lesser extent, NEUT-mAb alone (Fig. 4) showed lower expression of T cells and NK cell associated markers (*CD3d, CD3e, Klrc1, KLrd1, Lilrb4*) and cytotoxicity (*Gzma, Gzmb, Prf1*), as well as proinflammatory genes (*IL1a, Il1b, TNf, Ifng*)) and ISGs (*Cxcl10, Cxcl9, Cxcl11, Stat1*) (Fig. 4). Mice treated with non-neutralizing ADCC-mAb showed decreased expression of genes related to immune cell infiltration and inflammation, but expression levels of *granzymes, Ccl5, Fcgr4,* and *Ifnb* were similar to those of untreated mice (Fig. 4). Interestingly, despite the relatively higher levels of infiltrating immune cells detected in the eyes from polyAb-treated mice (Fig. 3), gene expression analysis showed overall reduction in the immune and inflammatory responses in the eyes of those animals except *Ccl5* and *Slamf7* (Fig. 4). Taken together, these findings suggest that the use of anti-EBOV antibodies reduces infection and mitigates immune and inflammatory responses albeit through different mechanisms.

Anti-EBOV-GP antibody treatment reduces VSV-EBOV-induced long-term ocular complications

Although EVD can cause ocular manifestations such as uveitis and hemorrhagic conjunctivitis in its acute phase, the convalescence phase also has been linked to serious ocular complications including uveitis with ocular redness and pain, cataracts, and vision loss.[6,11] To date, it remains unknown whether these long-term sequelae could be reduced in EVD survivors treated with the recently licensed antibodies to EBOV-GP. In a previous study, we established a sublethal-challenge mouse model to assess the long-term consequences of GP-mediated viral neurotropism by challenging neonatal mice with 500 TCID50 VSV-EBOV at P3, and showed that treatment of anti-EBOV-GP antibodies in these animals can reduce the neurological sequelae of the infection.[22] As previously reported, a sublethal-challenge of neonatal mice allows for 30–40% survival despite attaining similar viral burden in the eyes at the peak of infection (9 dpi) as the mice that receive a lethal dose (Fig. 5a and b). VSV-N RNA was amplified from the eyes of infected mice treated with IgG control (6 out of 6 mice), polyAb (2 out of 5 mice) and ADCC-mAb (5 out of 7 mice) at 3 mpi but not from those treated with NEUT-mAb or the combination of ADCC-mAb and NEUT-mAb (Fig. 5c). To confirm that viral RNA detected is not residual but represents replicating virus, we next tested for the presence of positive-sense RNA strands, which is considered indicative of ongoing replication. All the infected mice treated with IgG control had detectable levels of positive-sense RNA in the eyes, indicating the persistence of replicating viruses in the eyes in convalescent mice (Fig. 5d). The results confirmed that treatment with NEUT-mAb alone or together with ADCC-mAb was most effective at reducing the levels of viral RNA in the eyes at 3 mpi (Fig. 5c and d), whereas mice treated with polyAb or ADCC-mAb alone were positive for positive-sense RNA. Taken together, our findings suggest that mice challenged early with VSV-EBOV have a persistent reservoir in the eyes, and that viral clearance afforded by the different therapeutic antibodies differs (Fig. 5c and d).

Despite the presence of low levels of replicating viruses in the eyes, active retinal inflammation was not evident in convalescent mice. Histopathology of the eyes revealed the presence of neuroretinal destruction, photoreceptor loss, retinal folds, and cataracts in all IgG control-treated mice, indicating a previous occurrence of severe inflammation in the eyes (Fig. 5e). Fundus

eyes. Scale bar: 50 μm. Images of the full eye can be found in Supplementary Figure S6. **(d)** Flow cytometry analysis of cells isolated from the eyes collected at 9 dpi. The graphs show the percentage of infiltrating immune cells (CD45$^+$) and T cells (CD45$^+$CD3$^+$NK1.1$^-$) in the eyes from uninfected mice (n = 3) and VSV-EBOV-infected mice treated with IgG control (n = 5), polyAb (n = 4), ADCC-mAb (n = 7), NEUT-mAb (n = 5) or the combination of ADCC-mAb and NEUT-mAb (n = 5). Data are shown as mean + SD. *P < 0.05, **P < 0.01, ***P < 0.001 compared to uninfected mice. #P < 0.05 and ##P < 0.01 compared to VSV-EBOV-infected mice treated with IgG control.

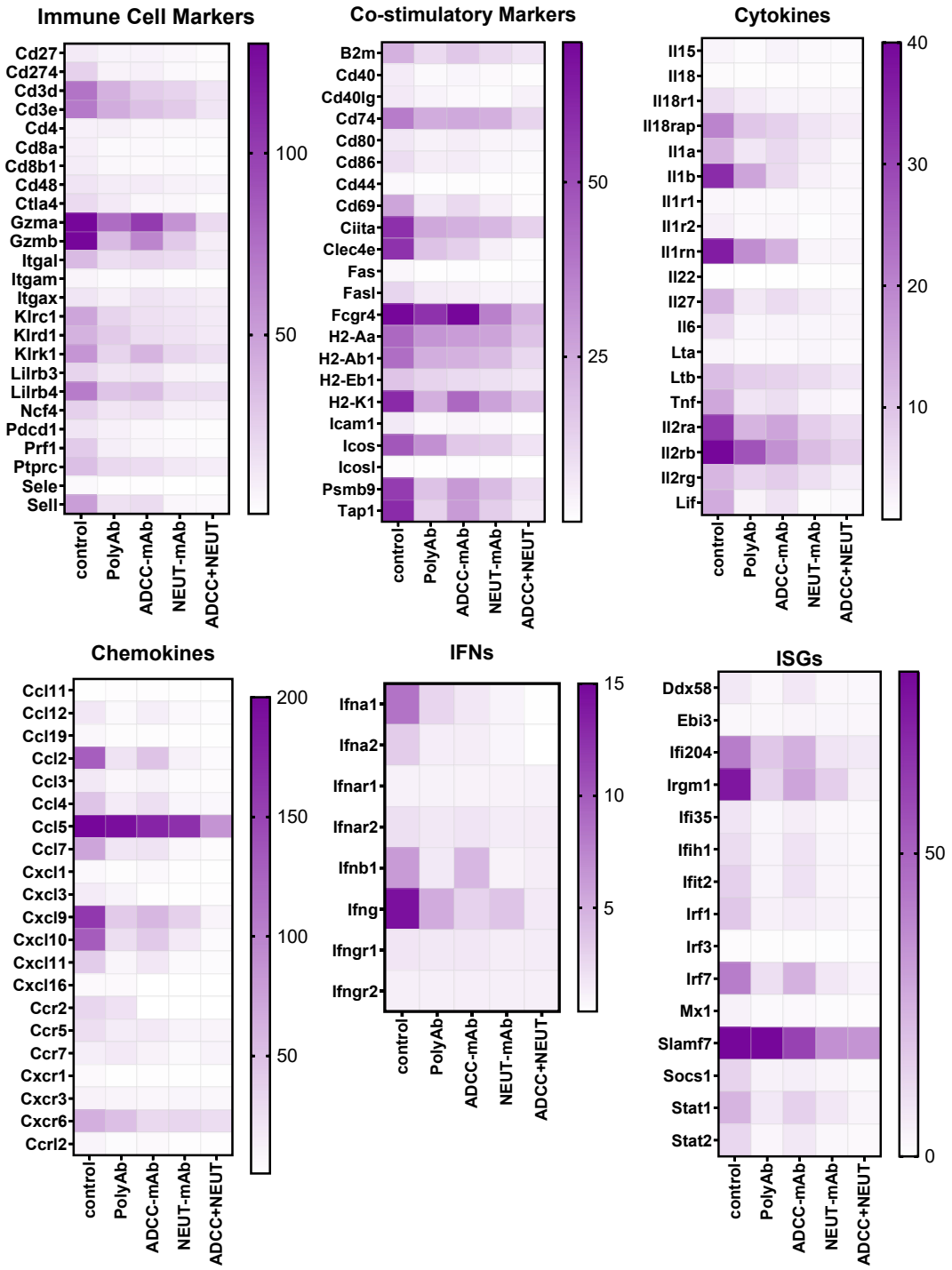

Fig. 4: **Pattern of inflammation in the eyes of VSV-EBOV-infected mice treated with IgG control or anti-EBOV-GP-antibodies**. Heat map of mRNA expression genes selected from a 591 gene array in the eyes at 9 dpi from VSV-EBOV-infected mice treated with IgG control (n = 8), polyAb (n = 7), ADCC-mAb (n = 3), NEUT-mAb (n = 3) or the combination of ADCC-mAb and NEUT-mAb (n = 3). RNA expression was assessed by NanoString using the nCounter mouse Immunology panel. Expression levels were normalized to the mean value of the uninfected group (n = 3). Results from the full gene array can be found in Supplementary Figure S7.

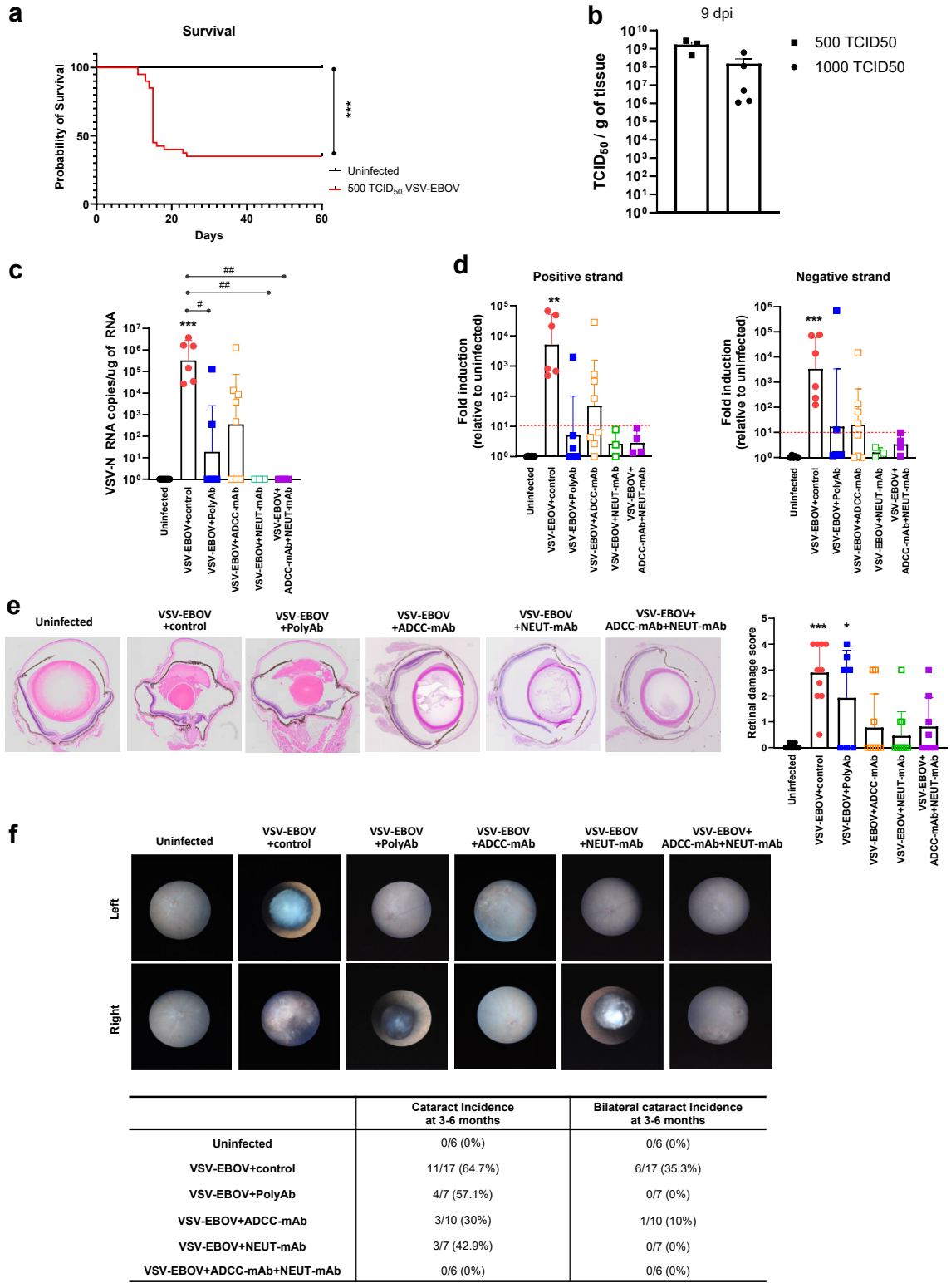

	Cataract Incidence at 3-6 months	Bilateral cataract Incidence at 3-6 months
Uninfected	0/6 (0%)	0/6 (0%)
VSV-EBOV+control	11/17 (64.7%)	6/17 (35.3%)
VSV-EBOV+PolyAb	4/7 (57.1%)	0/7 (0%)
VSV-EBOV+ADCC-mAb	3/10 (30%)	1/10 (10%)
VSV-EBOV+NEUT-mAb	3/7 (42.9%)	0/7 (0%)
VSV-EBOV+ADCC-mAb+NEUT-mAb	0/6 (0%)	0/6 (0%)

Fig. 5: **Sequelae of VSV-EBOV-infected mice treated with IgG control or anti-EBOV-GP antibodies**. **(a and b)** P3 neonatal mice were uninfected (n = 19) or infected s.c. with 500 TCID50 of VSV-EBOV (n = 42) and monitored for survival **(a)** for 60 days. Statistical significance was determined using the log-rank test. ***$P < 0.001$ compared to uninfected mice. **(b)** Comparison of viral load in the eyes from mice

examination also showed cataract development in 50% of eyes from infected mice while none of age-matched mice developed the cataract (Fig. 5f). As expected, treatment of ADCC-mAb, NEUT-mAb or their combination significantly reduced VSV-EBOV-induced retinal inflammation or damages in the long-term model. Interestingly, more than half of polyAb-treated mice (4 out of 7 mice) showed retinal sequela reminiscent of the damage observed in infected mice treated with IgG controls (Fig. 5e). However, all treatments with anti-EBOV-GP antibodies, including polyAb, reduced bilateral cataract development. The effect was most striking for the combination regimen, where none of infected mice developed cataract, suggesting that controlling infection by targeting EBOV-GP in the acute phase can minimize cataract development (Fig. 5f). Together, these data suggest that the sublethal challenge of VSV-EBOV can be used to model long-term ocular sequelae and compare the relative bioactivity of therapeutics targeting EBOV-GP.

Discussion

Patients, including children, who survive EVD have a high incidence of uveitis and cataracts with profound impact on their quality-of-life, and there is a concern regarding reinfection and transmission.[9,29] The development of therapeutic antibodies targeting the EBOV-GP have revolutionized the treatment of EVD by significantly improving the survival rates, broader questions of the role of therapeutic intervention in the human–filoviral interaction still need to be considered.[16] Many of the knowledge gaps for EBOV are rooted in the limitations of the available animal models including the need for BSL-4 animal facilities. In this study, we describe a BSL-2-compatible animal model that can be used to explore the dynamics of a replicating pseudovirus expressing the EBOV-GP in the eyes during both acute infection and in convalescence and can be used to compare the therapeutic effects of anti-EBOV-GP antibodies on both stages. Indeed, our study shows that although all of the therapeutic antibody preparations tested significantly reduced lymphopenia and weight loss and improved mouse survival, the magnitude of the effect in clearing the virus from the eyes and reducing long term pathology was markedly different. Since all the injected antibodies, including the non-specific IgG controls, were detectable in the eyes of infected mice 3 days post-treatment (Supplementary Figure S4), the differential effects of anti-EBOV-GP antibodies in clearing the virus from the eyes may be attributed to the distinct functions of each antibody preparation, rather than limitations in the accessibility of some therapeutics to immune-privileged sites.

Although EBOV outbreaks have occurred regularly since its identification in 1976, systematic follow-up of sequelae started only following the 2013–2016 outbreak that occurred in Western Africa, which left 11,000 patients dead and over 17,000 survivors. EVD survivors endure a wide variety of post-EVD sequelae including a high prevalence of uveitis (15–35%) and vision-threatening secondary ophthalmic complications including cataract, pupillary and epiretinal membranes, vitreoretinal traction, and retinal detachment.[7–9] Most studies suggest that in the long-term, the virus is not recovered from the aqueous humor sampled during pre-operative evaluations of EVD survivors with post-uveitis cataract. However, reports of persistent infections in immune-privileged sites, including a case of a patient with persistent infection 14 weeks after EVD although he had been treated with an experimental small interfering RNA anti-viral agent and convalescent plasma, hinder their integration in society and complicate their medical treatment as many of these patients require surgery to avoid blindness.[12]

To date, there is no detailed histopathology available to characterize EVD-associated clinical uveitis in humans, and this leads to some uncertainty regarding the management for antivirals and anti-inflammatories to reduce ocular sequela. Studies in animal models, particularly those aimed at assessing the long-term sequelae are very limited due to the requirement of animal biosafety level 4 settings and the dearth of susceptible immune competent rodent models. A study in ferrets reported viral RNA in the eye without histopathological findings,[30] whereas a study conducted in non-human primates indicated that the virus causes panuveitis with persistent vitreous haze and pupillary dysfunction with accumulation of T cells in the vitreous body,[13,31] which is closer to the pathology in humans. Here, we showed that neonatal C57BL/6 mice challenged with replication-competent VSV-EBOV pseudovirus

challenged with 500 TCID50 (n = 3) or 1000 TCID50 (n = 5) of VSV-EBOV by TCID50 analysis at 9 dpi. Data are shown as mean + SD. **(c–f)** P3 C57BL/6 mice were uninfected (n = 8) or infected with 500 TCID50 of VSV-EBOV and treated with IgG control (n = 6), polyAb (n = 6), ADCC-mAb (n = 8), NEUT-mAb (n = 3) or the combination of ADCC-mAb and NEUT-mAb (n = 4) at 3 dpi, and sacrificed at 3–6 months post infection (mpi). RNA from eyes of uninfected and convalescent mice was tested for the expression of VSV-N **(c)**, VSV-EBOV-positive sense RNA **(d, left)** and VSV-EBOV-negative sense RNA **(d, right)** in the eyes. Ct values normalized to housekeeping gene (GAPDH). Data are shown as mean + SD. The red dashed lines indicate the limit of detection. **(e)** Histopathology of the eyes at 3–6 mpi. Left images show representative H&E staining of eyes from uninfected mice (n = 9) and VSV-EBOV-infected mice treated with IgG control (n = 10), polyAb (n = 7), ADCC-mAb (n = 9), NEUT-mAb (n = 11) or the combination of ADCC-mAb and NEUT-mAb (n = 8). Right graph shows the retinal inflammation score. Data are shown as mean + SD. **(f)** Fundus images of the eyes showing cataract development at 3–6 mpi. Right table shows cataract incidence by eyes.

develop high levels of VSV-EBOV in the eyes, that are associated with retinitis, choroiditis and vitritis as well as lymphopenia during acute infection, before succumbing to the infection. By combining immunohistochemistry, histology, flow cytometry and gene expression profiles, we show that mouse eyes infected with VSV-EBOV have increased immune cell infiltration, apoptosis and microglial activation as well as upregulation of pro-inflammatory gene expression. While VSV-EBOV is a pseudovirus, its tropism is defined by the EBOV-GP on its envelope and therefore it targets the same tissues as EBOV. In the eye, this results in infection of multiple layers and cells of the retina including amacrine, horizontal, bipolar cells with clear damage to INL and photoreceptor layer as well as the retinal pigment epithelium (RPE) cells by 9 dpi. In contrast, while wild-type VSV infection displays broad CNS tropism including the eye, VSV-EBOV primarily localizes to the cornea, with minimal spread to other segments of the eye,[32] indicating that the cell tropism of VSV-EBOV is determined by EBOV-GP, and not VSV. Importantly, the use of a sublethal-challenge with the pseudovirus enables the study of the long-term consequences of the acute infection. In those mice, there is evidence of residual retinitis and unilateral or bilateral cataracts at 3–6 mpi that recall the sequelae observed in surviving patients. Importantly, in these mice we could detect not only negative-stranded RNA genome of EBOV, but also positive-stranded RNA. This suggests there is viable virus persistence in the eyes, even if the TCID50 assay performed on VERO E6 cells failed to detect replicating virus in the eyes of convalescent VSV-EBOV mice at 6 mpi (data not shown). This limitation might stem from the low sensitivity of TCID50, which fails to detect titers of the virus lower than 10^3 TCID50 units, as previously described.[24,33]

The increased susceptibility to neurotropic viruses including VSV-EBOV in neonatal mice and non-human primates has been well documented.[34,35] Our previous study also showed that immunocompetent adult mice are resistant to VSV-EBOV infection, whereas immunocompetent neonatal mice develop a productive symptomatic infection. Further, we showed that this is not necessarily linked to defective interferon responses but could be secondary to immature innate immune responses in neonates allowing unchecked virus proliferation.[24] A study from Basha et al. suggests that neonatal humans and mice have an inherent bias toward Th2-cell polarizing cytokines and suboptimal Th1 responses and B-cell differentiation, rendering neonates more susceptible to infections.[36] In addition, other factors such as the frequency of immature replicating cells, or the level of other anti-viral factors such as cholesterol 25-hydroxylase (CH25H) expression may contribute to the different susceptibility between neonates and adults.[37,38] While the model does not recapitulate every aspect of EVD, it can offer insight into determinants of susceptibility to infection and help confirm the role of biomarkers of populations at risk of developing ocular sequelae following VSV-EBOV infection. Further, it allows for assessment and comparison of anti-EBOV therapeutics. Lastly, since all the treatments tested result in animal survival, the model may offer clues as to the cells that harbor the virus long-term and can be used to examine the impact of therapeutics on ocular sequelae. As shown in Figs. 2–4, even when treated after the eyes were uniformly infected (3 dpi), the antibody-based treatments attained significantly different levels of viral clearance and consequent tissue damage. The neutralizing activity of the antibodies was critical for reducing retinal damage as mice treated with ADCC-mAb did not modify retinal disruption, cellular apoptosis, and inflammation. Interestingly, those treated with the polyAb preparation also appeared to have limited control of the virus, with significant apoptosis and high cellular infiltration. In contrast, the eyes of mice treated with a combination of ADCC-mAb and NEUT-mAb showed complete viral clearance, as well as limited apoptosis and cellular infiltration that resulted in reservation of retinal architecture. Of note, administration of a neutralizing mAb alone was not sufficient to completely clear the virus, but the damage to the retinal architecture was markedly reduced. The impact of the treatment on the acute disease was also evident long-term, as animals treated with the combination of ADCC-mAb and NEUT-mAb had minimal signs of chronic retinal inflammation and no evidence of virus persistence compared with those treated with polyAb or ADCC-mAb alone. The limited effect of ADCC-mAb on virus clearance during the acute phase was associated with viral persistence but not necessarily with ongoing inflammation in the eyes at 3–6 mpi. Conversely, mice treated with NEUT-mAb alone had no evidence of virus persistence, but the incidence of cataract development was comparable to those treated with polyAb or ADCC-mAb alone. These results underscore the importance of optimizing the interplay between neutralization capacity and immune modulation in ocular pathology. Further, the persistence of infection in some mice indicates that caution is needed in distinguishing the sequelae from acute damage from that due to persistent infection and possible continuous low-grade inflammation. Future studies will need to address this as it could hinder the interpretation of studies targeting residual infections. Similarly, the relatively reduced effectiveness of polyAb in controlling the acute infection or reducing ocular sequelae despite similar neutralization in vitro as well as 100% survival and reduced neurological damage was surprising.[22] Importantly, in this study all the treatments were dosed at 100 μg/kg in total; future dose–response studies with poly-IgG could demonstrate that the polyclonal product, when administered in high doses, could achieve similar level of reduction in eye pathology.

Indeed, this mouse model could be used to optimize the ratio of different therapeutics to maximize viral clearance and minimize tissue damage. Further, future studies will need to examine whether anti-EBOV-GP antibodies can be used to clear virus from eyes with persistent low-grade infection, as this would facilitate the treatment of patients that require surgery to address their ocular sequelae. Together these findings suggest that the BSL-2 compatible immune competent animal model offers a platform to help select therapeutic approaches that not only improve survival but also reduce ocular sequelae.

While it is likely that the therapeutic effect of anti-EBOV-GP antibodies is linked to systemic viral clearance, it is possible that therapeutic antibodies also play a role in the local clearance of virus. BRB is composed of the inner and outer BRB, and this static barrier serves to restrict drug delivery into the target site of eyes such as the posterior segment. The retinal capillary endothelial cells form the inner BRB, and RPE cells surrounded by choroidal capillaries make up the outer BRB.[39] Our studies and others show that RPE cells are highly susceptible to EBOV infection, and more importantly, are considered as potential reservoirs for EBOV in the eyes. *Ex vivo* studies in several different ocular tissues from cynomolgus monkey eyes indicated that RPE presents the most rapid EBOV growth kinetics and the highest end viral titers.[40] Also, *in vitro* study using ARPE-19 human ocular RPE cells supports that RPE allows EBOV replication and release in high titers.[41] In this study, viral antigen was evident in RPE and photoreceptor layer of the eye from VSV-EBOV-infected mice at 9 dpi suggesting a potential disruption of the BRB allowing for therapeutics given at 3 dpi to permeate the BRB. This is consistent with the detection of anti-EBOV-GP antibodies in the eye tissues following intraperitoneally injected although their role in local viral clearance could not be ascertained (Supplementary Figure S4).

Lymphopenia with T cell depletion represents a prevalent feature of EVD, and the degree of lymphopenia correlates strongly with mortality rates among EVD patients.[42] Several reports demonstrate that EBOV does not infect T lymphocytes but triggers T cell death by inducing cytokine storm through TLR4 or Tim-1 binding.[42,43] Similarly, in our animal model VSV-EBOV infection leads to lymphopenia with a marked decrease in lymphocytes and an inversion of the CD4:CD8 ratio, while mature myeloid cells including monocytes, neutrophils, basophils and eosinophils remain unaffected (Fig. 1d and Supplementary Figure S5). Concordant with the systemic changes in blood cell counts, treated mice showed relatively lower levels of macrophages infiltrating the eyes compared to infected untreated mice (37% vs 17–24%; Supplementary Figure S3d). The lymphopenia is reflected in the cell composition infiltrating the eye, which shows relatively lower levels of T cells in IgG control-treated mice compared to polyAb-treated mice (Fig. 3d and Supplementary Figure S3d) despite having higher number of total infiltrating cells than those treated with ADCC-mAb, NEUT-mAb or the combination. Since macrophages can not only support virus replication, but their infection results in dysregulated cytokine production and ensuing inflammation, this could underly the reduction in lesion severity among treated mice.[44]

Several reports indicate that EVD survivors often develop unilateral uveitis, cataract or vision loss.[45] Similarly, the sequela of infection in our model were not observed equally in both eyes, and this led to a significant variability within the groups as illustrated by the mice that developed cataracts. As shown in Fig. 5, a third of infected mice developed bilateral cataracts, while none of the mice treated with NEUT-mAb or the combination of ADCC-mAb and NEUT-mAb did, however almost half of the mice treated with NEUT-mAb alone developed unilateral cataracts. This underscores the necessity for a substantial sample size to comprehensively investigate the effects of therapeutics on ocular infection and pathology. Lastly, it should be mentioned that at 3–6 months post infection, the defects in the cornea hindered consistent assessment of the retina by fundoscopy. Future studies may need to develop improved methods of visualizing the retina in convalescent mice.

In summary, our data describes a new immune competent animal model that can be used to improve our understanding of EBOV-GP-mediated ocular disease and screen candidate therapeutics targeting EBOV-GP under BSL-2 conditions. While the utilization of VSV-EBOV-GP, rather than wildtype EBOV, does not support comprehensive genomic analyses or the identification of potential mutations or defective interfering particles associated with persistence in ocular tissues, the study provides valuable insights into the differential therapeutic potential of anti-EBOV-GP antibodies that target EBOV suggesting that not all the therapeutics that improve survival similarly reduce ocular complications. The differential effects of different antibody treatments on viral clearance, pathology, inflammation, and long-term complications in the eyes highlight the importance of antibody selection and improved understanding of host–pathogen interactions. This model should aid in target selection and optimization to improve the outcome of patients affected in future outbreaks.

Contributors

HL, ILM, MM and DV designed the study; HL mainly performed the experiments and analyzed the data; BX performed fundus examination and analyzed the data; APL, KE and DDCI helped with the experiments; LKB helped with statistical analysis; JLK, JL and RNF performed immunocytochemistry and analyzed the images; MMC helped with H&E staining; CCC analyzed H&E images; AB, CK and KP provided antibodies and helped with ADCC assay; HL, RRC and DV discussed the data; HL wrote the manuscript; MM and DV revised the manuscript. All authors read and approved the final version of the manuscript.

Data sharing statement

All raw data in the study will be made available from the lead contact upon any reasonable request.

Declaration of interests

All authors have read and confirmed the manuscript and accepted the responsibility to submit it for publication. The authors declare that they have no known competing financial interests or personal relationships that could have appeared to influence the work reported in this paper.

Acknowledgements

This manuscript reflects the views of the author and should not be construed to represent FDA's views or policies. We thank John Dennis, Ruth Molano, and the personnel of the animal facility for care of the mice. Also, we thank Christian Sauder, Marjorie Shapiro and Susan Kirshner for reviewing the manuscript, and SAB Biotherpeutics, Inc for providing antibodies.

Appendix A. Supplementary data

Supplementary data related to this article can be found at https://doi.org/10.1016/j.ebiom.2024.105170.

References

1 Murray MJ. Ebola virus disease: a review of its past and present. *Anesth Analg*. 2015;121(3):798–809.
2 Kadanali A, Karagoz G. An overview of Ebola virus disease. *North Clin Istanb*. 2015;2(1):81–86.
3 Gao JW, Guo ZY, Li W, Zhang XW, Zhang XE, Cui ZQ. Ebola virus disrupts the inner blood-retinal barrier by induction of vascular endothelial growth factor in pericytes. *PLoS Pathog*. 2023;19(1):e1011077.
4 Feldmann H, Geisbert TW. Ebola haemorrhagic fever. *Lancet*. 2011;377(9768):849–862.
5 Leligdowicz A, Fischer WA 2nd, Uyeki TM, et al. Ebola virus disease and critical illness. *Crit Care*. 2016;20(1):217.
6 Burki TK. Post-Ebola syndrome. *Lancet Infect Dis*. 2016;16(7):780–781.
7 Tiffany A, Vetter P, Mattia J, et al. Ebola virus disease complications as experienced by survivors in Sierra Leone. *Clin Infect Dis*. 2016;62(11):1360–1366.
8 Hebert EH, Resnikoff S, March L, Delaporte E. Ocular complications in survivors of the ebola outbreak in Guinea REPLY. *Am J Ophthalmol*. 2017;181:180.
9 Eghrari AO, Bishop RJ, Ross RD, et al. Characterization of ebola virus-associated eye disease. *JAMA Netw Open*. 2021;4(1):e2032216.
10 Shantha JG, Canady D, Hartley C, et al. Ophthalmic sequelae and psychosocial impact in pediatric ebola survivors. *eClinicalMedicine*. 2022;49:101483.
11 Berry DE, Li AL, Yeh S, Shantha JG. Ocular complications in Ebola virus disease survivors: the importance of continuing care in West Africa. *Expert Rev Ophthalmol*. 2019;14(3):179–185.
12 Varkey JB, Shantha JG, Crozier I, et al. Persistence of ebola virus in ocular fluid during convalescence. *N Engl J Med*. 2015;372(25):2423–2427.
13 Worwa G, Cooper TK, Yeh S, et al. Persistent intraocular Ebola virus RNA is associated with severe uveitis in a convalescent rhesus monkey. *Commun Biol*. 2022;5(1):1204.
14 Taki E, Ghanavati R, Navidifar T, Dashtbin S, Heidary M, Moghadamnia M. Ebanga (TM): the most recent FDA-approved drug for treating Ebola. *Front Pharmacol*. 2023;14:1083429.
15 Rayaprolu V, Fulton BO, Rafique A, et al. Structure of the Inmazeb cocktail and resistance to Ebola virus escape. *Cell Host Microbe*. 2023;31(2):260–272.e7.
16 Iversen PL, Kane CD, Zeng XK, et al. Recent successes in therapeutics for Ebola virus disease: no time for complacency. *Lancet Infect Dis*. 2020;20(9):E231–E237.
17 Aschenbrenner DS. Monoclonal antibody approved to treat ebola. *Am J Nurs*. 2021;121(4):22.
18 Hansen F, Feldmann H, Jarvis MA. Targeting Ebola virus replication through pharmaceutical intervention. *Expert Opin Investig Drugs*. 2021;30(3):201–226.
19 Liu J, Trefry JC, Babka AM, et al. Ebola virus persistence and disease recrudescence in the brains of antibody-treated nonhuman primate survivors. *Sci Transl Med*. 2022;14(631):eabi5229.
20 Jain S, Martynova E, Rizvanov A, Khaiboullina S, Baranwal M. Structural and functional aspects of ebola virus proteins. *Pathogens*. 2021;10(10):1330.
21 Lee JE, Saphire EO. Ebolavirus glycoprotein structure and mechanism of entry. *Future Virol*. 2009;4(6):621–635.
22 Lee HN, McWilliams IL, Lewkowicz AP, et al. Characterization of the therapeutic effect of antibodies targeting the Ebola glycoprotein using a novel BSL2-compliant rVSVDeltaG-EBOV-GP infection model. *Emerg Microb Infect*. 2021;10(1):2076–2089.
23 Saito T, Maruyama J, Nagata N, et al. A surrogate animal model for screening of ebola and marburg glycoprotein-targeting drugs using pseudotyped vesicular stomatitis viruses. *Viruses*. 2020;12(9):923.
24 McWilliams IL, Kielczewski JL, Ireland DDC, et al. Pseudovirus rVSVDeltaG-ZEBOV-GP infects neurons in retina and CNS, causing apoptosis and neurodegeneration in neonatal mice. *Cell Rep*. 2019;26(7):1718–1726.e4.
25 Manangeeswaran M, Ireland DDC, Verthelyi D. Zika (PRVABC59) infection is associated with T cell infiltration and neurodegeneration in CNS of immunocompetent neonatal C57Bl/6 mice. *PLoS Pathog*. 2016;12(11):e1006004.
26 Caspi RR, Roberge FG, Chan CC, et al. A new model of autoimmune disease. Experimental autoimmune uveoretinitis induced in mice with two different retinal antigens. *J Immunol*. 1988;140(5):1490–1495.
27 Coleman JW, Ogin-Wilson E, Johnson JE, et al. Quantitative multiplex assay for simultaneous detection of the Indiana serotype of vesicular stomatitis virus and HIV gag. *J Virol Methods*. 2007;143(1):55–64.
28 Iampietro M, Younan P, Nishida A, et al. Ebola virus glycoprotein directly triggers T lymphocyte death despite of the lack of infection. *PLoS Pathog*. 2017;13(5):e1006397.
29 Shantha JG, Crozier I, Yeh S. An update on ocular complications of Ebola virus disease. *Curr Opin Ophthalmol*. 2017;28(6):600–606.
30 Watson RJ, Tree J, Fotheringham SA, et al. Dose-dependent response to infection with ebola virus in the ferret model and evidence of viral evolution in the eye. *J Virol*. 2021;95(24):e0083321.
31 Zeng X, Blancett CD, Koistinen KA, et al. Identification and pathological characterization of persistent asymptomatic Ebola virus infection in rhesus monkeys. *Nat Microbiol*. 2017;2:17113.
32 Pollikoff R, DiPuppo A, Cannavale P. Vesicular stomatitis virus (VSV) infection in rabbit eye: role of antibody and interferon. *Invest Ophthalmol*. 1969;8(5):488–496.
33 Ireland DDC, Manangeeswaran M, Lewkowicz AP, et al. Long-term persistence of infectious Zika virus: inflammation and behavioral sequela in mice. *PLoS Pathog*. 2020;16(12):e1008689.
34 Garbutt M, Liebscher R, Wahl-Jensen V, et al. Properties of replication-competent vesicular stomatitis virus vectors expressing glycoproteins of filoviruses and arenaviruses. *J Virol*. 2004;78(10):5458–5465.
35 Geisbert TW, Daddario-Dicaprio KM, Lewis MG, et al. Vesicular stomatitis virus-based ebola vaccine is well-tolerated and protects immunocompromised nonhuman primates. *PLoS Pathog*. 2008;4(11):e1000225.
36 Basha S, Surendran N, Pichichero M. Immune responses in neonates. *Expert Rev Clin Immunol*. 2014;10(9):1171–1184.
37 Mallard C, Ek CJ, Vexler ZS. The myth of the immature barrier systems in the developing brain: role in perinatal brain injury. *J Physiol*. 2018;596(23):5655–5664.
38 Meljon A, Theofilopoulos S, Shackleton CH, et al. Analysis of bioactive oxysterols in newborn mouse brain by LC/MS. *J Lipid Res*. 2012;53(11):2469–2483.
39 Varela-Fernandez R, Diaz-Tome V, Luaces-Rodriguez A, et al. Drug delivery to the posterior segment of the eye: biopharmaceutic and pharmacokinetic considerations. *Pharmaceutics*. 2020;12(3):269.
40 Matson MJ, Bushmaker T, Scott DP, et al. Ebola virus tropism in ex vivo cynomolgus macaque ocular tissues. *J Infect Dis*. 2023;228(Suppl 7):S626–S630.
41 Smith JR, Todd S, Ashander LM, et al. Retinal pigment epithelial cells are a potential reservoir for ebola virus in the human eye. *Transl Vis Sci Technol*. 2017;6(4):12.
42 Younan P, Santos RI, Ramanathan P, et al. Ebola virus-mediated T-lymphocyte depletion is the result of an abortive infection. *PLoS Pathog*. 2019;15(10):e1008068.
43 Younan P, Iampietro M, Nishida A, et al. Ebola virus binding to tim-1 on T lymphocytes induces a cytokine storm. *mBio*. 2017;8(5):e00845.
44 Wanninger TG, Millian DE, Saldarriaga OA, et al. Macrophage infection, activation, and histopathological findings in ebolavirus infection. *Front Cell Infect Microbiol*. 2022;12:1023557.
45 Vetter P, Kaiser L, Schibler M, Ciglenecki I, Bausch DG. Sequelae of Ebola virus disease: the emergency within the emergency. *Lancet Infect Dis*. 2016;16(6):e82–e91.